Energy Transfer in a Nanoscale Multichromophoric System: Fluorescent Dye-Doped Conjugated Polymer Nanoparticles

Changfeng Wu, Yueli Zheng, Craig Szymanski, and Jason McNeill*

Department of Chemistry and Center for Optical Materials Science and Engineering Technologies, Clemson University, Clemson, South Carolina 29634

Received: May 29, 2007; In Final Form: November 26, 2007

We report on the fluorescence properties and the combined effects of energy diffusion and energy transfer in polyfluorene nanoparticles doped with a variety of fluorescent dyes. As the doping host, polyfluorene possesses extraordinary "light harvesting" ability, resulting in higher per-particle brightness as compared to dye-loaded silica nanoparticles of similar dimensions. Both the steady-state fluorescence spectra and time-resolved fluorescence measurements indicate highly efficient energy transfer from the host polymer to the acceptor dye molecules. A model that takes into account the combined effects of energy diffusion, Förster transfer, and particle size was developed. Comparisons of experimental data to the model results elucidate the importance of particle size and energy diffusion within the polymer in determining the optical properties of the doped conjugated polymer nanoparticles. Fluorescence quantum yields of ∼40% and peak extinction coefficients of 1.5×10^9 $M^{-1}cm^{-1}$ were determined for aqueous suspensions of ∼30 nm diameter polymer nanoparticles doped with perylene or coumarin 6 (2 wt %). Photobleaching experiments indicate that energy transfer phenomena strongly influence the photostability of these dye-doped nanoparticles. Significant features of these nanoparticles include the high brightness, highly red-shifted emission spectrum, and excellent photostability, which are promising for biological labeling and sensing applications. In addition, the nanoparticles are a useful model system for studying energy transfer in dense, nanostructured, multichromophoric systems.

1. Introduction

Förster resonance energy transfer (FRET), a physical phenomenon in which energy absorbed by a fluorophore is transferred to another molecule through a nonradiative pathway,[1] has experienced a resurgence of interest due to a number of emerging applications such as molecular beacon biosensors[2,3] and optoelectronic devices.[4] Many conjugated polymers are known to possess high absorption coefficients and high fluorescence quantum efficiency.[5−7] In electroluminescent devices, energy transfer has been widely employed as a strategy for tuning the emission color and enhancing the quantum efficiency,[8] and a number of detailed investigations of device properties and photophysics of conjugated polymer thin films doped with various chromophores have been performed.[9−11] Additionally, energy transfer is the basis for the FRET technique used for studying short-range (<10 nm) interactions between biomolecules and conformational changes.[12−15] Conjugated polymers demonstrate great potential for application in highly sensitive biosensors based on extraordinarily efficient energy transfer phenomena characterized as superquenching or hyperquenching.[16,17] We have recently demonstrated the possibility of using hydrophobic conjugated polymer nanoparticles as fluorescent probes.[18,19] Highly efficient energy transfer was observed in blended conjugated polymer nanoparticles[19] and between conjugated polymer nanoparticles and Au nanoparticles.[18] Although conventional Förster theory is typically adequate for describing energy transfer from a single fluorescent donor to a single acceptor (or an ensemble of independent acceptors), dense multichromophoric systems such as conjugated polymers consist of multiple donors that are highly coupled, resulting in mobile excitons. Application of the Förster theory to these systems may require significant modification in the theory.[20]

Highly fluorescent probes such as nanoparticles have attracted much attention due to a number of demanding applications such as biosensing, imaging, and high throughput assays.[21,22] As compared to conventional fluorescent dyes, inorganic semiconductor quantum dots and dye-loaded beads exhibit improved brightness and photostability and are under active development for fluorescence-based biological applications.[23−25] Quantum dots are ideal probes for multiplexed assays due to their broad excitation band and narrow, tunable emission peaks. However, cytotoxicity is of concern for in vivo applications.[26,27] Energy transfer has been exploited in the design of fluorescent dyes and polymers[28,29] and has also been used to improve the functionalities of dye loaded latex or silica colloids. Some commercially available beads incorporate a series of two or more dyes that undergo excited energy transfer and exhibit a highly red-shifted emission spectrum. Triple-dye-doped silica nanoparticles have been demonstrated in which FRET-mediated emission features could be tuned by varying the doping ratio of the three tandem dyes.[30] However, the relatively large particle sizes (>30 nm) of these and other doped silica particles may preclude sensing applications involving the use of energy transfer to report conformational changes (e.g., molecular beacons).

Many conjugated polymers have high fluorescence quantum yields and broad emission spectra with full widths at half-

* To whom correspondence should be addressed. E-mail: mcneill@clemson.edu.

10.1021/jp074149+ CCC: $40.75
Published on Web 01/24/2008

maximum (fwhm) of ~50−100 nm, meeting the requirements for an efficient, versatile donor. Conjugated polymers also possess extraordinary "light harvesting" ability due to their large extinction coefficients and also exhibit very fast intra- and interchain photoexcitation transport (exciton diffusion). These characteristics offer possible advantages for the development of novel fluorescent nanoparticles. In this study, we report on the fluorescence and energy transfer photophysics of polyfluorene nanoparticles doped with a variety of fluorescent dyes. The doped polyfluorene nanoparticles exhibit fluorescence excitation spectra characteristic of the host polymer and fluorescence emission spectra characteristic of the dopant dyes. These doped nanoparticles are many times brighter than inorganic quantum dots and dye-loaded silica particles of similar dimensions—in one case, a nanoparticle fluorescence quantum yield of ~40% and a peak extinction coefficient of 1.5×10^9 $M^{-1}cm^{-1}$ were determined for particles with an average diameter of 30 nm. The high experimentally observed energy transfer efficiency is not adequately described by Förster energy transfer alone. A model was developed that includes the combined effects of exciton diffusion, Förster transfer, and particle size in determining the energy transfer efficiency. Comparisons of experimental results to the results of simulations based on the model yielded an exciton diffusion length within the range of accepted literature values. The model was also used to explore the effects of particle size on intra-particle energy transfer efficiency. These nanoparticles could serve as a model system for studying energy transfer in complex nanoscale systems consisting of densely packed chromophores. An improved understanding of the photophysics in such systems would be of benefit for enhancing the performance of nanoparticle-based sensing schemes and nanostructured electroluminescent device layers.

2. Experimental Section

2.1. Materials. The polyfluorene derivative poly(9,9-dihexylfluorenyl-2,7-diyl) (PDHF, MW 55 000, polydispersity 2.7) was purchased from ADS dyes (Quebec, Canada). The fluorescent dyes perylene, nile red, and tetraphenylporphyrin (TPP), and the solvent tetrahydrofuran (THF, anhydrous, 99.9%) were purchased from Sigma-Aldrich (Milwaukee, WI). Coumarin 1, Coumarin 6, and [2-[2-[4-(dimethylamino)phenyl]ethenyl]-6-methyl-4H-pyran-4-ylidene]-propanedinitrile (DCM) were purchased from Exciton (Dayton, OH). All chemicals were used without further purification.

2.2. Nanoparticle Preparation. Preparation of the fluorescent dye-doped PDHF nanoparticles is performed using a method similar to the reprecipitation method described previously.[18,19,31] Dye-doped PDHF nanoparticles were prepared as follows. The PDHF polymer was dissolved in THF by stirring overnight under inert atmosphere. The solution was then filtered through a 0.7 micron filter and further diluted to a concentration of 40 ppm. A given fluorescent dye (either perylene, coumarin 6, nile red, or TPP) was also dissolved in THF to make a 100 ppm solution. Varying amounts of a dopant dye solution were mixed with a PDHF solution to produce solution mixtures with a constant host concentration of 40 ppm and dopant/host fractions ranging from 0 to 10 wt %. The mixtures were agitated to form homogeneous solutions. A 2 mL quantity of the solution mixture was added quickly to 8 mL of deionized water while sonicating the mixture. The resulting suspension was filtered through a 0.2 micron membrane filter. The THF was removed by partial vacuum evaporation, followed by filtration through a 0.2 micron filter. The resulting nanoparticle dispersions are clear and stable for months with no signs of aggregation.

2.3. Characterization Methods. Morphology and size distribution of the doped and undoped PDHF nanoparticles were characterized by atomic force microscopy (AFM) and transmission electron microscopy (TEM). For the AFM measurements, one drop of the nanoparticle dispersion was placed on a freshly cleaned glass substrate. After evaporation of the water, the surface topography was imaged with an Ambios Q250 multimode AFM in AC mode. Samples for TEM imaging were prepared by drop casting the nanoparticle dispersion onto copper grids. The samples were allowed to dry at room temperature, and then the TEM images were obtained using a Hitachi H-7600 microscope operated at 120 kV.

The UV−vis absorption spectra were recorded with a Shimadzu UV-2101PC scanning spectrophotometer using 1 cm quartz cuvettes. The fluorescence spectra were obtained using a commercial fluorometer (Quantamaster, PTI, Inc.). Photobleaching measurements were performed using methods similar to the those described elsewhere,[32] but using the light source built in the fluorometer. The slit widths on the excitation monochromator of the fluorometer were adjusted slightly to generate continuous UV light (380 nm) with a power of 1.0 mW as determined by a calibrated photodiode (Newport model 818-sl). The light was focused into a quartz cuvette containing a constantly stirred nanoparticle dispersion with an absorbance of 0.10. The fluorescence intensity at a specific wavelength was recorded continuously over a time period of 2 h. Fluorescence lifetimes were measured using the time-correlated single-photon counting technique (TCSPC). The sample was excited by the second harmonic (400 nm) of a mode-locked femtosecond Ti:Sapphire laser (Coherent Mira 9000). The output of a fast PIN diode (Thorlabs, DET210) monitoring the laser pulse was used as the start pulse for a time-to-amplitude converter (TAC, Canberra Model 2145). Fluorescence signal was collected in perpendicular geometry, passed through a 420 nm interference filter with a 10 nm bandwidth, and detected by a single photon counting module (Perkin-Elmer, SPCM-AQR). The output of the detector was used as the stop pulse for the TAC. The laser was attenuated to maintain the count rate below 20 kHz. The signal from the TAC was digitized using a multichannel analyzer (FastComTec, MCA-3A). The instrument response function was measured before and after each fluorescence lifetime measurement using the scattered laser light from a dilute suspension of polystyrene beads. The combination of the detector and electronics results in an instrument response function with a width of ~1.0 ns (fwhm).

3. Results and Discussion

3.1. Nanoparticle Size and Morphology. Previously, we reported a facile method for preparation of a variety of hydrophobic conjugated polymer nanoparticles.[18,31] The preparation involves a rapid mixing of a dilute solution of polymer dissolved in a water-miscible organic solvent with water. The rapid mixing with water leads to a sudden decrease in solvent quality, resulting in the formation of a suspension of hydrophobic polymer nanoparticles. It is possible to introduce hydrophobic fluorescent dyes during nanoparticle formation. Here, a variety of fluorescent dyes were chosen as dopant species based on their fluorescent quantum yield and spectral overlap with the donor's emission. Figure 1a presents the chemical structures of the dyes and PDHF polymer employed in this study. The doping concentration and the possibility of dye leakage were investigated by the following procedure. A nanoparticle suspension in which the nanoparticles contain 9 wt % of coumarin 6 and 91% of PDHF were prepared as

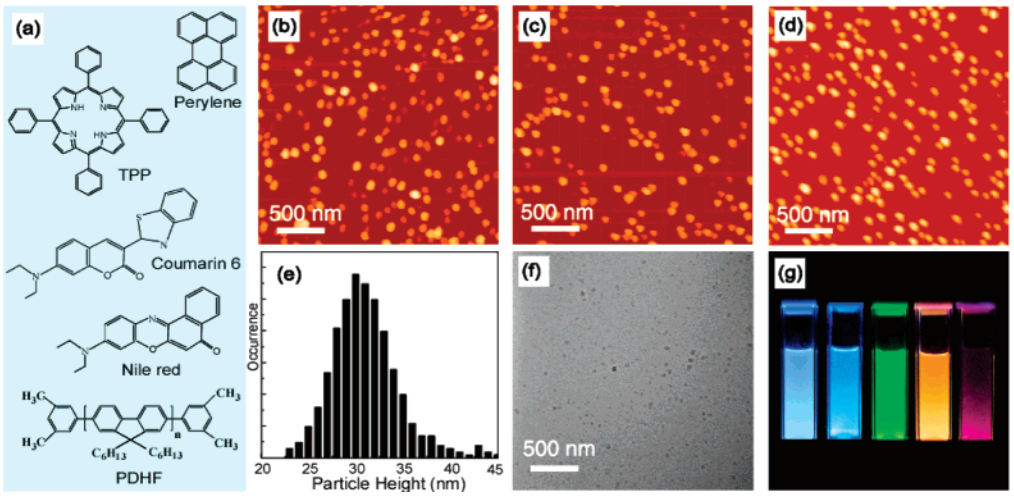

Figure 1. (a) Chemical structures of the fluorescent dye dopants and the host conjugated polymer PDHF. Representative AFM images of pure (b), perylene-doped (c), and coumarin 6-doped (d) PDHF nanoparticles dispersed on silica substrate. (e) Histogram of particle height data taken from AFM image (b). (f) TEM image of the pure PDHF nanoparticles. (g) Photograph of fluorescence emission from aqueous suspensions of the dye-doped PDHF nanoparticles taken under UV lamp excitation (365 nm). The composition and spectroscopy of these nanoparticles are indicated in Figure 3.

described in the previous section. The dye to polymer ratio in the nanoparticles was determined by UV−vis absorption spectroscopy, indicating that the dye to polymer ratio of the nanoparticle precursor mixture is preserved in the resulting nanoparticle suspension (i.e., neither species was preferentially precipitated during the preparation procedure). The overall preparation yield of the dye-doped nanoparticles was typically higher than 80%. To determine whether the dye was located primarily within the nanoparticles or as free dye molecules in solution, a series of tests were performed on the nanoparticle suspension as follows. The sample was concentrated by a factor of 6 using centrifugal concentrators (Pall Corp.) with a molecular weight cutoff of 30 000. A negligible absorption and very weak fluorescence from coumarin 6 were observed in the filtrate, which indicates that nearly all of the dye was embedded within the nanoparticles, with only a negligible fraction present as free dye in solution. The concentrated sample was diluted and the above procedure was repeated a few weeks later. The results indicate no observable dye leakage. The nanoparticle dispersions were drop-cast onto silica substrates for analysis of particle size and morphology by AC mode AFM. A representative AFM image of undoped PDHF nanoparticles is shown in Figure 1b. A particle height analysis obtained from the AFM image indicates that most particles possess diameters in the range of 30 ± 5 nm (Figure 1e). The lateral dimensions from the AFM image are somewhat larger than the height due to the radius of curvature of the AFM tip.[33] The size and morphology were also characterized by TEM (Figure 1f), which indicated well-dispersed, spherical nanoparticles with diameters of ∼30 nm. Our observations are consistent with the recent report that the equilibrium shape for small sized PDHF nanoparticles (∼30 nm) tends to be spherical because polymer−water interfacial tension is the dominant factor which typically determines the polymer morphology in this size range, even for somewhat rigid polymers such as PDHF.[34] There are estimated 100−300 polymer molecules per nanoparticle, assuming a densely packed spherical morphology. As shown in Figure 1c and 1d, the perylene-doped and coumarin 6-doped PDHF nanoparticles were characterized by AFM. Height analysis indicates that the presence of dopant has no apparent effect on particle size and morphology.

3.2. Fluorescence Spectroscopy. As a promising class of conjugated polymers for organic light-emitting devices, many

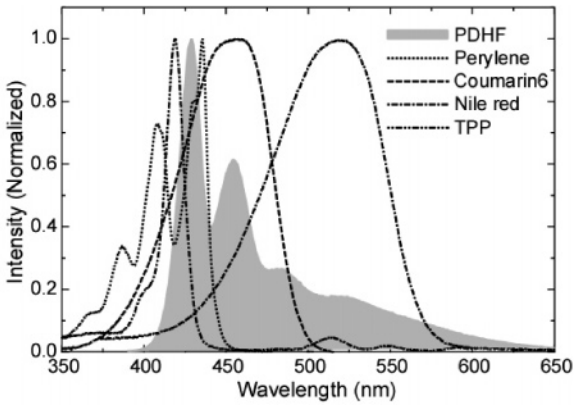

Figure 2. Normalized fluorescence emission spectrum of PDHF nanoparticles and absorption spectra of the fluorescent dyes.

polyfluorene derivatives exhibit blue emission with high fluorescence quantum yield.[6,7] In this study, PDHF was chosen as the host polymer in view of its high absorptivity in the near-ultraviolet region and broad emission spectrum which provides favorable spectral overlap with a number of different dopant species. Figure 2 presents the normalized fluorescence emission spectrum of the PDHF nanoparticles in water and absorption spectra of perylene, coumarin 6, nile red, and TPP in THF solutions. The fluorescence of the host polymer PDHF in ∼400−550 nm range possesses good overlap with the absorption spectra of the fluorescent dye molecules, as required for efficient energy transfer via the Förster mechanism. Figure 1g shows the strong fluorescence emission from aqueous suspensions of undoped and various doped PDHF nanoparticles under UV excitation (365 nm). At a few percent doping fraction, the fluorescence from PDHF is almost completely quenched and the nanoparticles present strong fluorescence from the dopant species, indicating efficient energy transfer from the host polymer to dopant molecules.

Figure 3 shows the normalized absorption (dashed curves), fluorescence excitation and emission spectra (solid curves) of the undoped PDHF and four dye-doped nanoparticles containing varying concentrations of perylene, coumarin 6, nile red, and TPP. The dominant absorption peaks (around 375 nm) of the

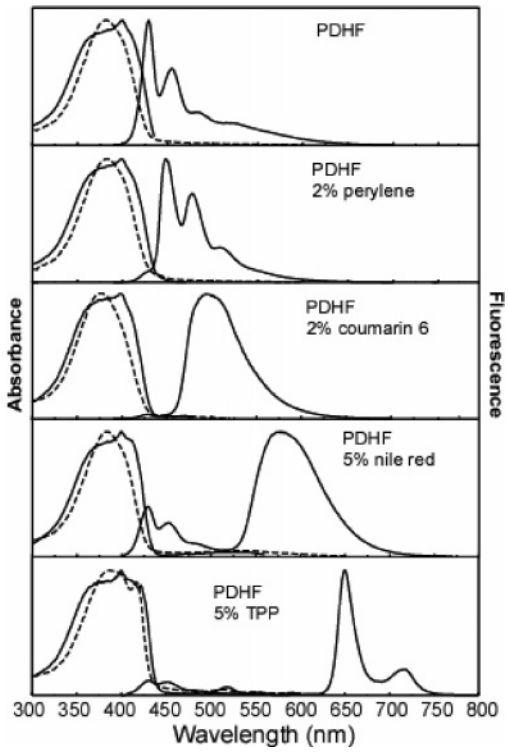

Figure 3. Normalized absorption (dashed), fluorescence excitation and emission spectra (solid) of pure and dye-doped PDHF nanoparticles.

dye-doped nanoparticles are due to PDHF, whereas relatively weak absorption from the dopant molecule can also be observed. With 375 nm excitation, where >95% of the absorption is due to PDHF, the fluorescence from PDHF is almost completely quenched, and the nanoparticles exhibit fluorescence emission spectra characteristic of the dopant species. Fluorescence excitation spectra obtained while monitoring dopant emission are very similar to the normalized absorbance spectra of PDHF, with minor differences attributable to the spectrum of the Xe lamp of the fluorometer. These observations indicate efficient intra-particle energy transfer from the PDHF host to the dopant fluorescent dyes. The observed energy transfer efficiencies are roughly similar to the energy transfer efficiencies observed for dye-doped polyfluorene thin films,[11,35,36] supporting the conclusion that the nanoparticles consist of polymers essentially in the solid state with dye molecules randomly distributed throughout the polymer.

Highly efficient energy transfer is evident in the evolution of the fluorescence spectra with increasing dopant concentration. Figure 4 shows the fluorescence emission spectra of the three types of dye-doped nanoparticles as dopant concentration is increased. For the case of PDHF nanoparticles doped with coumarin 6, the fluorescence from the PDHF host decreases with increasing dye content, whereas fluorescence from the dye increases and reaches a maximum around 1.0 wt %, after which a further increase in dopant concentration causes a pronounced reduction in fluorescence intensity. Over the concentration range of ~0.2−1 wt %, the nanoparticles present an intense green emission (~500 nm) from coumarin 6, which is clearly more intense than the 430 nm emission of undoped PDHF nanoparticles. It is also clearly observed that the green emission from coumarin 6 consists of two emission peaks around 500 nm. Very similar spectral features were observed in coumarin 6-doped polyfluorene and PVK thin films.[37] As the doping concentration is increased from 2 to 5 wt %, the intensity of the dye emission starts to drop and the spectra change shape, consistent with the

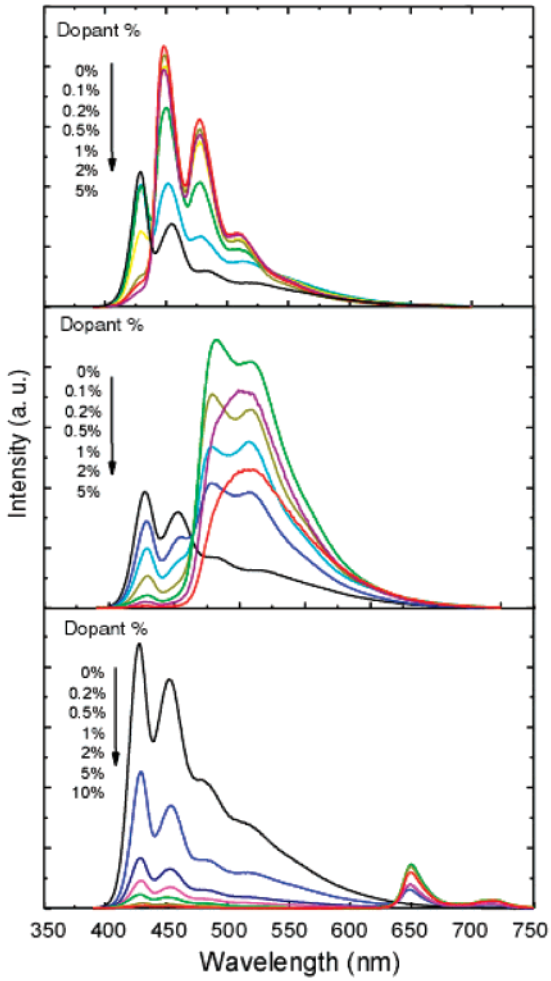

Figure 4. Concentration dependent fluorescence spectra of PDHF nanoparticles doped with perylene (top), coumarin 6 (middle), and TPP (bottom).

formation of dye aggregates with low fluorescence quantum yield. The perylene-doped system shows a similar trend in the evolution of the fluorescence as the fraction of dye is increased, but no additional spectral features from the perylene due to aggregation were observed, nor was quenching due to aggregates observed. The TPP-doped particles have a lower overall fluorescence quantum yield as compared to the other doped particles, consistent with the lower quantum yield of TPP as compared to coumarin 6 and perylene. Although we have successfully demonstrated the doping strategy for a few fluorescent dyes, it should be noted that acceptor emission was not observed for some other dyes. For the nile red-doped case, nanoparticles prepared with 5 wt % doping exhibit moderate fluorescence from the PDHF host, as indicated in Figure 3. The donor's fluorescence is not completely quenched even in more heavily doped samples (10 wt %). Another dye, DCM, was observed to quench the host fluorescence, but no obvious fluorescence from the dye was observed. This is somewhat contradictory to other reports on DCM-doped nanoparticles and thin films.[38−40] However, the results support the tentative conclusion that the rigid, nonpolar polymer matrix would inhibit formation of the twisted intramolecular charge transfer state considered to be the dominant fluorescence pathway for DCM.[41]

The dependence of the PDHF fluorescence intensity on the dye concentration was modeled using the Stern−Volmer relation, which can be expressed as[42]

$$F_0/F = 1 + K_{SV}[A] \quad (1)$$

where F_0 and F are fluorescence intensities in the absence and presence of acceptor, respectively, K_{SV} is the Stern−Volmer quenching constant, and [A] is the concentration of the acceptor. The quenching constant is obtained from the slope of a linear fit to a plot of F_0/F versus [A]. If the acceptor concentration is expressed as a molecule fraction, then K_{SV} represents the number of host molecules quenched by a single acceptor. The integrated emission intensities (F_0 and F) of the donor were obtained by decomposing the spectra in Figure 4 through a multi-peak Gaussian fitting. The Stern−Volmer analysis (Figure 5) indicated that approximately 3, 8, and 9 polymer molecules can be quenched by single molecules of perylene, coumarin 6, and TPP, respectively. The differences in the quenching efficiency per molecule can be attributed to the differences in the Förster radii of the three dyes. The perhaps surprising observation that a single dye molecule can quench one or more polyfluorene chains consisting of tens to hundreds of chromophore units is supported by a number of recent experimental reports that indicate that energy diffusion via rapid intrachain energy transfer is an important factor in determining energy transfer efficiency to acceptor dyes.[28,43] In the following sections, we attempt to quantify the relative importance of energy diffusion and Förster transfer by comparing experimental results to the results of simulations which include both energy diffusion and Förster transfer phenomena within the framework of a random walk.

3.3. Förster Energy Transfer Model. The Förster theory of resonance energy transfer is best understood by considering a single donor and acceptor separated by a distance R. The energy transfer rate constant (k_{ET}) with the donor−acceptor separation R is given by[42]

$$k_{ET} = \frac{\phi_D \kappa^2}{\tau_D R^6}\left(\frac{9000(\ln 10)}{128\pi^5 N_A n^4}\right)\int_0^\infty F_D(\lambda)\epsilon_A(\lambda)\lambda^4 d\lambda \quad (2)$$

where ϕ_D and τ_D are the fluorescence quantum yield and lifetime of the donor, respectively, in absence of the acceptor; κ^2 is a configurational factor describing the relative orientation of transition dipoles of the donor and acceptor and is usually assumed to be 2/3 for a random distribution of donor−acceptor pairs; N_A is Avogadro's number; n is the refractive index of the medium; $F_D(\lambda)$ is the normalized emission spectra of the donor; and $\epsilon_A(\lambda)$ is the molar absorption coefficient of the acceptor. It is convenient to define a distance R_0 (the Förster radius) at which the energy transfer rate constant k_{ET} is equal to the total decay rate constant ($k_{ET} = \tau_D^{-1} = k_R + k_{NR}$) of the donor in absence of the acceptor. Förster radii for the three dyes using PDHF as the donor were calculated using eq 2. Since the PDHF refractive index is strongly dependent on wavelength over its emission range, the wavelength-dependent refractive index was adopted for the calculation.[36,44] The spectral overlap between PDHF emission and dye absorption is presented in Figure 2. A fluorescence quantum yield of 20% was obtained for the PDHF nanoparticles using a solution of Coumarin 1 in ethanol as a standard.[45] The calculated Förster radii are 2.29, 3.05, and 3.14 nm for PDHF doped with perylene, coumarin 6, and TPP, respectively. The larger Förster radius of TPP is reflected by its large peak absorption coefficient (4.1×10^5 $M^{-1}cm^{-1}$) as compared to Coumarin 6 (5.4×10^4 $M^{-1}cm^{-1}$) and perylene (3.8×10^4 $M^{-1}cm^{-1}$). Coumarin 6 has a moderate molar absorption coefficient but very good spectral overlap; therefore, its Förster radius is comparable to that of TPP. As is clear from a comparison to the Stern−Volmer analysis, acceptors with larger Förster radii exhibit higher quenching efficiencies.

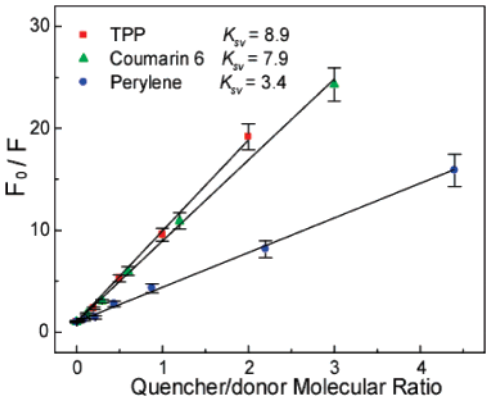

Figure 5. Fluorescence quenching of the donor versus molar fraction of quenchers in the dye-doped PDHF nanoparticles. The scattered points are experimental results of PDHF fluorescence quenched by the three dye acceptors, while the solid lines represent fits to the Stern−Volmer equation.

There have been a number of recent studies of energy transfer processes in dye-doped polyfluorene thin films.[11,35,36,46] The results were interpreted based on a model that assumes that dye molecules are arranged on a perfect cubic lattice within the polymer host. The lattice model is not appropriate for the nanoparticle systems currently under study because the quenching efficiency of the acceptors close to the surface is likely to be different from those close to the center of the particle. Furthermore, the dye molecules are likely to be more or less randomly distributed in the polymer host, which leads to a number of dye molecules with overlapping Förster radii, particularly at higher dye-to-polymer ratios. To address these issues, we have developed a method for estimating energy transfer efficiency that takes into account the random distribution of the donor and acceptor positions within the confined space of a nanoparticle. The model is described as follows: Assuming that the overall energy transfer rate constant (k_{ET}') scales linearly with the number of quenchers, the k_{ET}' from a randomly positioned exciton to all the quenchers can be expressed as

$$k_{ET}' = \sum_j^{N_A} k_{ET,j} = \sum_j^{N_A} \frac{1}{\tau_D}\left(\frac{R_0}{R_j}\right)^6 \quad (3)$$

where N_A is the number of dye molecules per particle, R_j represents the distance between the exciton and the jth dye molecule. Defining quenching efficiency q for a given exciton as $q = k_{ET}'/(k_R + k_{NR} + k_{ET}')$, the overall quenching efficiency Q can be calculated by averaging over a large number N_D of randomly generated exciton positions:

$$\frac{F_0 - F}{F_0} = Q = \frac{1}{N_D}\sum_i^{N_D} \frac{k_{ET,i}'}{1 + k_{ET,i}'} \quad (4)$$

Due to the sensitivity of the simulation results on the positions of the acceptors, the simulation results must be averaged over many randomly generated sets of acceptor positions as well. This simulation describes only the Förster energy transfer without considering exciton diffusion. The results of the simulations (using Förster radii calculated from the spectral overlap) and comparisons to experimentally determined quench-

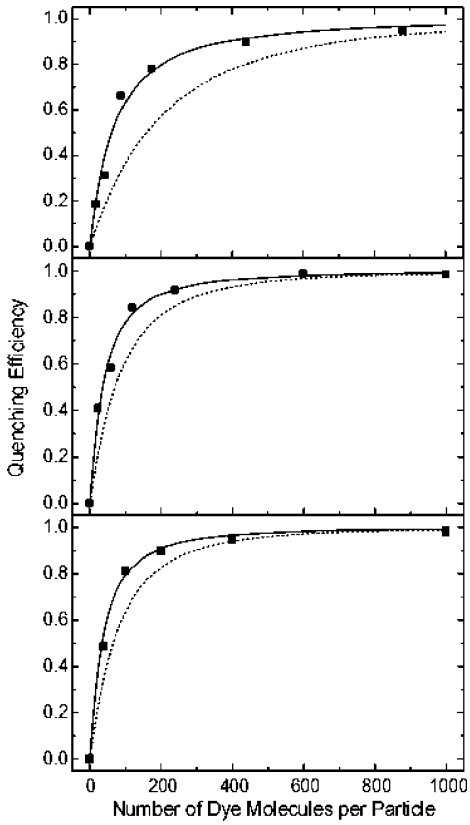

Figure 6. Quenching efficiency as a function of the number of dye molecules per particle for the PDHF nanoparticles doped with perylene (top), coumarin 6 (middle), and TPP (bottom). The squares are experimental results. The dotted curves represent the results of the Förster transfer model, while the solid curves represent the results of the combined exciton diffusion and Förster transfer model.

ing efficiencies are shown in Figure 6. We elected to use experimental measurements of donor emission quenching as a measure of energy transfer efficiency instead of using acceptor emission, because the latter is not a reliable indicator of energy transfer efficiency due to possible quenching by aggregate species. The scattered data show the experimental results for the three dyes calculated from Figure 4, whereas the dotted curves represent the simulation results using the Förster transfer model. Large discrepancies between the experimental and simulated quenching efficiencies (as high as 50%) were observed for all three dye species, which indicates that Förster transfer alone is not able to adequately account for the observed quenching behavior in these dye-doped nanoparticles and that other processes are likely to be involved, such as energy diffusion. Excitons in conjugated polymers can migrate along the polymer chain and may hop between chains, processes characterized by an exciton diffusion length, typically on the order of 5−20 nm for conjugated polymers.[46−48] Simulations of energy transfer that neglect energy diffusion are expected to underestimate the efficiency of energy transfer for such π-conjugated systems, as observed.

3.4. Combined Exciton Diffusion and Förster Transfer Model. Energy transfer from a conjugated polymer to fluorescent dyes is described as occurring in two steps:[11,36,43,46] (1) energy diffusion within the polymer host and (2) energy transfer from the host to the guest dye molecules. On the basis of the above picture, we introduce a model that explicitly takes into account the combined effects of exciton diffusion, energy transfer, and particle size. The model is based on a 3D random walk on a discrete cubic lattice. Random walk-based methods have been previously employed to model exciton diffusion and trapping in molecular crystals.[49,50] However, the present model differs significantly from these previous models in that the possibility of Förster energy transfer to an acceptor dye is taken into account for each step in the random walk trajectory. The model and simulation methods are described as follows: The exciton is given an initial random position within the nanoparticle. After a time interval of duration Δt, the exciton moves a single step of length ϵ in a random direction, subject to the constraints imposed by the geometry of the particle. Neglecting (for the moment) energy transfer to the dye acceptors, the average number of steps N required for the exciton to travel a distance equal to the exciton diffusion length L_D is given by $N = (L_D/\epsilon)$.[2] The time step size Δt is related to the fluorescence lifetime of the donor (τ_D) by $N\Delta t = \tau_D$. A given number of acceptor dye molecules are randomly distributed within a nanoparticle. At each step, the overall energy transfer rate constant k_{ET}' is calculated based on the position of the exciton and the positions of the acceptors according to eq 3. The probabilities of energy transfer and decay during the time step are calculated as $p = 1 - \exp(-k_{ET}'\Delta t)$ and $p = 1 - \exp(-\Delta t/\tau_D)$, respectively. Comparison of generated random numbers against the probabilities of the two processes is used to determine if the exciton has undergone decay or transfer during the time step, ending the trajectory. If not, the exciton trajectory continues to the next step. Each trajectory is allowed to eventually terminate in either energy transfer or decay. The algorithm was verified by comparison of simulation results (obtained with energy transfer turned off) with the analytical expression for steady-state concentration as a function of distance for a decaying species which is diffusing from a point source.[51] It should be noted that, for materials with an optical penetration depth similar to that of the particle radius, the initial distribution of excitons (prior to energy diffusion) would be more heavily weighted toward the surface. However, this is not of major concern in the present case, because the particle radius is a factor of 2−3 smaller than the optical penetration depth.

A comparison of the model results to the experimentally determined quenching efficiencies was performed as follows: The number of acceptor dyes per particle used in the simulations was varied over the range of 0−1000, consistent with the range of experimental data. The same Förster radii used in the previous section were employed for the combined energy diffusion and transfer model. The exciton diffusion length was treated as a fit parameter and evaluated over the range of 6−10 nm. The step length ϵ was set to a value of 0.1 nm. Values for ϵ between 0.05 and 0.5 nm were found to yield similar quenching efficiency results, indicating little sensitivity to this parameter provided that it is set to a value well below the Förster radius and the exciton diffusion length. Thousands of exciton trajectories were calculated, and the quenching efficiency was determined by counting the number of trajectories that terminate in energy transfer relative to the total number of trajectories. The efficiencies were also averaged over many random acceptor positions, because the energy transfer efficiency is sensitive to the random placement of acceptors. For a given average number of acceptors per nanoparticle, the actual number of acceptors per nanoparticle is likely to follow a Poisson distribution. However, Poisson statistics were neglected because it was previously determined that it does not affect the average quenching efficiency for cases where the quenching efficiency per acceptor is below 30%.[19] A comparison of the calculated energy transfer efficiencies for a range of diffusion length values to the experimental results (Figure 6) yields an estimated exciton

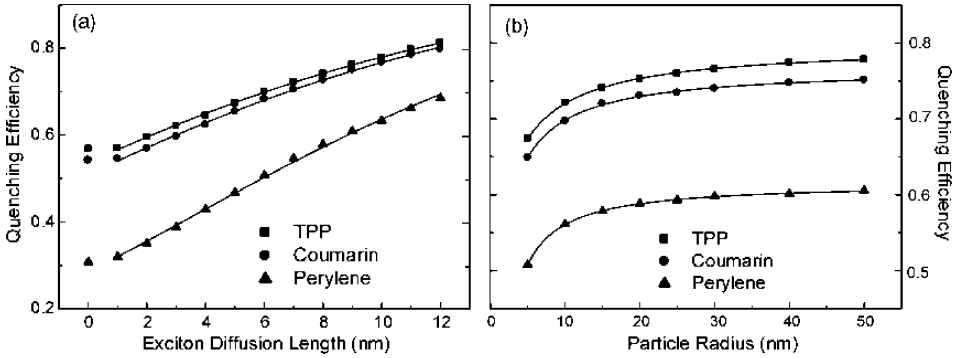

Figure 7. (a) Dependence of the quenching efficiency on the exciton diffusion length for the three dye-doped nanoparticles. The starting points in the absence of exciton diffusion were calculated according to eq 4, whereas the other points were obtained by the combined energy diffusion and Förster transfer model. The curves are fits to eq 6. (b) Size dependent quenching efficiency for the particles doped the three different dye species. The number of dye molecules per unit volume is fixed at a value of 0.0057 per nm^3, corresponding to 80 dye molecules in a particle with a radius of 15 nm. The scattered points are simulation results, and the curves merely serve as guides to the eye.

diffusion length parameter of 8 ± 1 nm for all three dyes. The agreement between theory and experiment is quite good over a large range of dye concentrations. An exciton diffusion length of 8 nm is consistent with reported values for similar materials, which range from 4 to 20 nm.[46,52,53] The excellent agreement between the model and experimental results, as compared to the model results obtained without energy diffusion, provides a strong indication of the importance of energy diffusion in this system. An additional issue that should be considered is whether the model assumption that the dyes are positioned randomly is physically reasonable. Entropic considerations and the particle formation kinetics associated with rapid mixing would tend to favor the assumption that dye positions are essentially random. However, depending on the particular dye species, surface free energy could be minimized by segregation of the dye on the surface. Because segregation of the dyes on the surface cannot be ruled out, it is appropriate to consider the effect of such segregation on the quenching efficiency of the dyes and the relative importance of energy diffusion and energy transfer. This issue can be addressed on a qualitative level as follows. If a dye molecule is located on the surface, this would reduce the effective quenching volume of the dye, because about half of the volume defined by the Förster radius of the dye would intersect with the particle. Indeed, simulations in which the dyes were confined to the surface resulted in substantially smaller quenching efficiencies (as much as a factor of 2 smaller) as compared to the results obtained assuming a random dye distribution within the entire volume of the particle. Thus, a larger exciton diffusion length parameter would be required to obtain agreement between the model and the experimental results. On the basis of these considerations, the exciton diffusion length obtained from the comparison between the model results and the experimental results should be taken as a lower estimate of the exciton diffusion length.

Additional simulations were conducted to explore the dependence of quenching efficiency on the exciton diffusion length. For 80 dye molecules per nanoparticle, the quenching efficiency was determined as a function of exciton diffusion length (Figure 7a). The points corresponding to $L_D = 0$ were calculated according to eq 4, whereas the other points were obtained using the combined energy diffusion and Förster transfer model. As can be seen, the quenching efficiency increases monotonically with increasing the exciton diffusion length, approaching unity for L_D values well above the particle size (data not shown). A parametrized expression that takes into account both energy transfer and exciton diffusion was developed as follows. We define an effective energy transfer radius R_{ET} similar to the Förster radius, assuming that R_{ET} depends approximately linearly on the exciton diffusion length (L_D),

$$R_{ET} = R_0 + \alpha \cdot L_D \tag{5}$$

where α is a parameter describing the relative contribution of exciton diffusion to the effective energy transfer radius. Replacing R_0 of conventional Förster theory with the effective energy transfer radius, the quenching efficiency can be written as

$$Q = \frac{(R_0 + \alpha \cdot L_D)^6}{\bar{R}^6 + (R_0 + \alpha \cdot L_D)^6} \tag{6}$$

where $\bar{R}$ represents an effective average distance from a donor to the nearest acceptor. Figure 7a shows the fitting curves to the results of by setting $\bar{R}$ and α as parameters. Fits to the combined energy diffusion and transfer simulations yielded excellent fits for all three dye species using parameters in the range of $\bar{R} = 3.0 \pm 0.2$ nm and $\alpha = 0.064 \pm 0.001$. The effective energy transfer distance (including energy diffusion) is only 15−20% larger than R_0, when using L_D values of 8 nm. There is uncertainty of similar magnitude in typical R_0 values determined from spectral overlap. This indicates the necessity of careful determination of Förster radii as well as the need to obtain additional data for validation such as by systematically varying the acceptor concentration and employing a variety of acceptors.

To explore the dependence of quenching efficiency on nanoparticle size, simulations were performed using the combined energy diffusion and Förster transfer model (Figure 7b). For each particle size, number of dye molecules per unit volume is fixed at a value of 0.0057 per nm^3, corresponding to 80 dye molecules for a particle with a radius of 15 nm. As can be seen, the quenching efficiency increases monotonically for small particles in the radius range of ~5−25 nm, approaching constant values for particle radii above 30 nm. The reason for this size dependence can be interpreted as follows: for smaller particles, the dopant molecules are more likely to be located close to the surface due to the higher surface to volume ratio. The dye molecules near the surface have a smaller effective quenching volume as compared to those farther from the surface (nearer the particle center), leading to a lower quenching efficiency. As particle radius increases, the surface effect is relatively less significant, and therefore the quenching efficiency increases. For cases in which the particle radius is above 30 nm, well above the Förster radius, the quenching efficiency approaches

a constant value corresponding to the bulk solid. The radii of the prepared dye-doped PDHF particles (~13−17 nm) is well below the estimated ~30 nm threshold for bulk quenching behavior, indicating that particle size is an important factor in this case. The apparent size dependence of the energy transfer properties of the nanoparticles points to the possibility of tuning energy transfer parameters using particle size or other nanoscale geometric parameters.

Time-resolved fluorescence measurements were performed to provide detailed information about energy transfer rate constants. Fluorescence decay kinetics traces were obtained using the TCSPC technique. Donor excited-state lifetimes were extracted from the kinetics traces using custom software employing an iterative deconvolution method.[54] Statistical analysis of several fits and comparison of lifetime results obtained for Coumarin 6 in ethanol to literature values yields an estimated uncertainty in the reported lifetime of 50 ps or better. A fluorescence lifetime of 330 ps was obtained from the decay curves of the 420 emission of the undoped PDHF nanoparticles. This is consistent with reported lifetimes for similar polyfluorene derivatives that range from 160 to 400 ps in thin films.[11,36] An increase in the decay rate of PDHF fluorescence is observed as the TPP concentration is increased. For the 0.2 wt % doped sample, the energy transfer rate constant ($k_{ET}^{'}$) was deduced by subtracting the decay rate constant of undoped nanoparticles ($\tau_D^{-1} = 3.0\ ns^{-1}$) from the total decay rate constant of the doped nanoparticles ($\tau_D^{-1} = 5.5\ ns^{-1}$). The result ($k_{ET}^{'} = 2.5\ ns^{-1}$) is consistent the value calculated using the combined energy diffusion and Förster transfer model. The decay time (100 ps) from a more heavily doped sample (0.5 wt %) indicates a clear enhancement of energy transfer rate constant ($k_{ET}^{'} = 7.0\ ns^{-1}$) due to the higher dopant concentration and is also consistent with the results of the simulations. It should be noted that the experimental time resolution was insufficient to observe the complex dynamics that are often observed in systems involving energy transfer to randomly distributed acceptors.[46,55] Additional experiments with improved time resolution are planned in order to address this question.

3.5. Photobleaching Behavior of the Dye-Doped Nanoparticles. The photostability of fluorescent nanoparticles is of critical importance for many fluorescence sensing and imaging applications. The photostability of a fluorescent dye or nanoparticle can be characterized by photobleaching quantum yield (ϕ_B), which is equal to the number of molecules that has been photobleached divided by the total number of photons absorbed over a given time interval.[32] In other words, photobleaching quantum yield is the reciprocal of the number of excitation cycles that a typical molecule endures before it undergoes irreversible photobleaching and can be expressed as

$$\phi_B = \frac{k_B}{k_R + k_{NR} + k_{ET} + k_B} \tag{7}$$

where k_B is the photobleaching rate constant usually related to photochemical reactions involving the excited-state of the molecule. Conventional fluorescent dyes such as coumarins and rhodamines typically exhibit bleaching quantum yields in the range of $\sim 10^{-4}-10^{-6}$.[32] For typical fluorescent dyes under low excitation intensity, the photobleaching kinetics follows a single-exponential decay curve. However, the photobleaching of conjugated polymers is more complicated, and the mechanism remains poorly understood due to the complex set of interactions involving a large number of species such as excitons, polarons, molecular oxygen, and partially oxidized species of unknown structure.[56] Polyfluorene-based thin films in air often exhibit spectral instability that involves the appearance of an undesired green emission arising from energy transfer to a small number of keto (fluorenone) defects resulting from partial oxidation of the polymer.[57] Similarly, partially oxidized PDHF nanoparticles exhibit green emission due to the presence of fluorenone sites on the polymer backbone. Figure 8a shows the emission spectra of the 0.5% TPP-doped PDHF nanoparticles before and after 2 h of photobleaching under 380 nm UV light. A comparison between the spectra exhibits clearly an increased green emission around 530 nm, whereas the emission intensities from the polyfluorene host (430 nm) and the TPP guest (650 nm) are reduced. The photobleaching kinetics data for doped and undoped PDHF nanoparticles are shown in Figure 8b. The photobleaching kinetics of the undoped PDHF particles cannot be described by a single-exponential decay. However, the sum of two exponential functions, with a fast component characterized by a time constant of 600 s (30%) and a slow component characterized by a time constant 3.0×10^4 s (70%), adequately reproduces the photobleaching curve. The observed biexponential photobleaching kinetics could indicate the presence of two or more distinct populations, possibly due to the presence of different phases with distinct morphology and photophysics. It has previously been observed that different phases of polyfluorene derivatives can be prepared from the same polymer, each with markedly different fluorescence and electronic properties arising from differences in the nanostructure of the material.[7,58] The observation of multiple decay rates is also consistent with

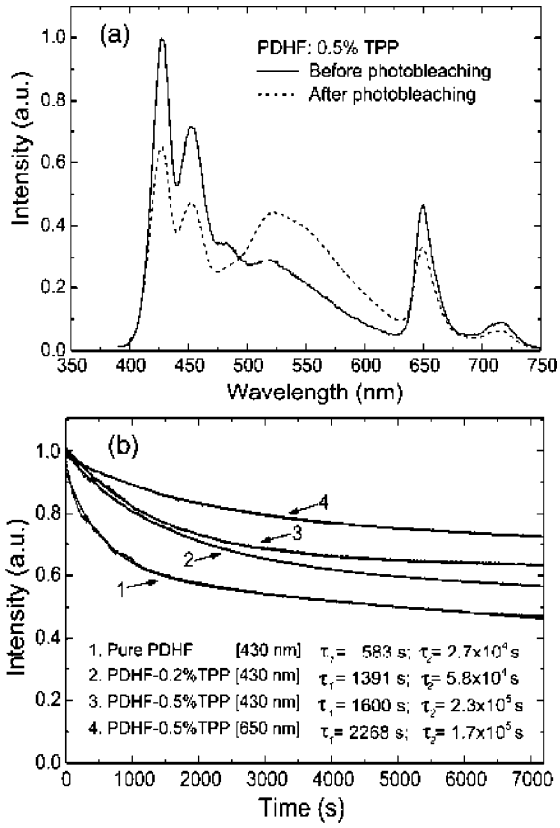

Figure 8. (a) Fluorescence emission spectra of TPP-doped PDHF (0.5%) before and after 2 h of photobleaching. (b) Photobleaching kinetics of the pure and TPP-doped PDHF nanoparticles under continuous illumination with 1.0 mW of 380 nm UV light. The absorbance of the samples was 0.10. The wavelengths in brackets indicate the emission collection wavelengths. The black curves result form the fitting by double exponential decay and the time constants are indicated in the Figure.

the possibility that chains located near the surface of the particle could be more susceptible to photobleaching as compared to chains located deeper within the nanoparticle. Another possibility is that the combination of energetic disorder and intraparticle energy transfer results in energy transfer from higher energy excitations to states of lower energy. This results in a range of excited-state lifetimes, which would give rise to multiexponential photobleaching kinetics, according to eq 7. A procedure similar to that described by Eggeling and co-workers[32] was employed to obtain quantitative photobleaching quantum yields from the photobleaching kinetics data. To validate the procedure, analysis of photobleaching kinetics for Coumarin 6 was performed, yielding results similar to reported values.[32] The fast bleaching component corresponds to a photobleaching quantum yield of 1.0×10^{-6}, whereas the slow bleaching component corresponds to a photobleaching quantum yield of 2.6×10^{-8}. Because the fraction of emitted photons associated with the rapidly decaying component is very small, the determination of death number (ϕ_F/ϕ_B) is based on the fluorescence quantum yield ($\phi_F = 0.20$) and the slow photobleaching component ($\phi_B = 2.6 \times 10^{-8}$), yielding a death number of 7.7×10^6 photons per undoped PDHF nanoparticle.

We also determined the effect of energy transfer on photostability of the doped nanoparticles. TPP was chosen as the dopant due to its highly red-shifted fluorescence which provides clear separation between donor and acceptor fluorescence. Biexponential fits to the photobleaching kinetic traces of 0.2 wt % TPP-doped nanoparticles of doped particles yield time constants of 1391 s for the fast-bleaching component and 5.8×10^4 s for the slow component in the host photobleaching kinetics, both approximately a factor of 2 larger than the time constants obtained for undoped particles. Recalling the results from a previous section, the energy transfer efficiency is approximately 50% at the doping fraction of 0.2 wt % TPP. According to the rate picture, an energy transfer efficiency of 50% would reduce the photobleaching rate constant by a factor of 2 as compared to undoped nanoparticles, consistent with the observed photobleach kinetics. A higher dopant ratio (0.5 wt % TPP) leads to longer time constants for both the two components. Again, this is consistent with the rate picture (eq 7). During the course of the photobleaching kinetics measurement, light also bleaches the dopant molecules (Figure 8b), which should result in partial recovery of donor fluorescence, though this phenomenon had no apparent effect on the photobleaching kinetics. The photobleaching kinetics of the acceptor emission at 650 nm emission of the 0.5%TPP-doped sample exhibits a biexponential decrease similar to that of the donor. Regarding the death number for doped nanoparticles, the calculation indicates the death number for the donor's fluorescence is roughly the same to that of the pure PDHF nanoparticles because the lower photobleaching rate is offset by the lower donor quantum yield. However, there is a net increase in total death number per particle when the emission from the acceptors is included. In the 0.5%TPP-doped sample, the death number for the acceptor's fluorescence is calculated to be 3.2×10^6 photons per nanoparticle according to the fluorescence quantum yield ($\phi_F = 0.013$) and the photobleaching kinetic trace ($\phi_B = 4.1 \times 10^{-9}$) of the acceptors. The death number of the nanoparticle (considering acceptor emission only) is similar to that of free TPP in solution multiplied by the number of dye molecules per nanoparticle ($\sim$100). Extrapolating to the case of heavily doped nanoparticles (negligible donor emission and short donor lifetime), the nanoparticle death number would be largely determined by the number of acceptor molecules multiplied by the acceptor death number. Because dye loading fractions similar to those typically employed in dye-loaded silica or polystyrene nanospheres can be achieved with the dye-loaded PDHF particles, we tentatively conclude that similar photostability figures of merit could be achieved. On the basis of these results, we conclude that doping with energy acceptors is a viable strategy for improving photostability of conjugated polymer nanoparticles.

It has been observed that, in some cases, the photobleaching rate is proportional to the triplet state population of the fluorophores,[59] and that triplets can result in complex photobleaching kinetics.[59,60] If the dopant species are able to act as triplet quencher, it would increase the photostability of the donor. Similarly, oxygen is potent triplet quencher and has been found to increase the fluorescence intensities of conjugated polymers.[61] In addition, singlet oxygen generated by interaction of O_2 with triplet states is also likely to be involved in the production of partially oxidized defect species. Although TPP is known to be an efficient singlet oxygen generator, and singlet oxygen is known to be involved in photobleaching, we observed no reduction in the photostability of TPP-doped particles as compared to undoped particles.

Finally, we consider the nanoparticle figures of merit for fluorescence labeling applications. We previously observed that the conjugated polymer nanoparticles suffered from a reduction in fluorescence quantum yield as compared with the polymers in organic solvent.[18] Blended conjugated polymer nanoparticles were developed later and found to have a slightly higher quantum yield.[19] The dye-doping strategy provides additional options for optimizing nanoparticle optical properties due to the wide range of readily available dyes with quantum yields approaching unity. Furthermore, PDHF as host has efficient light harvesting ability as compared to optically inert polymer or silica materials. Nearly all of the excitation energy absorbed by hundreds of PDHF molecules is transferred to the dye acceptors, which can exhibit a high fluorescence quantum yield. The combination of large per-particle absorptivity and high fluorescence quantum yield results in large improvements in fluorescence brightness. Fluorescence quantum yields of $\sim$40% and a peak extinction coefficient of 1.5×10^9 $M^{-1}cm^{-1}$ (assuming 200 polymer molecules for a nanoparticle with 30 nm diameter) were determined for PDHF nanoparticles doped with perylene or coumarin 6 (2 wt %) suspended in water, using a solution of Coumarin 1 in ethanol as a standard.[45] Another significant feature of the dye-doped nanoparticles is their highly red-shifted emission spectrum as compared to pure polymers and typical fluorescent dyes. Differently doped nanoparticles with a variety of emission wavelengths can be simultaneously excited using a single light source, a useful feature for imaging and multiplexed fluorescence detection. Photostability is also an important factor for many applications. We observed that the dye molecules in the PDHF particles have photostability similar to that of free dyes in solution, as estimated from the photobleaching experiments. Because each particle contains hundreds of dyes, the death numbers and survival times of the dye-doped nanoparticles appear to be hundreds times better than single conventional molecular dyes and similar to dye-loaded polymer spheres of similar dimensions. On the basis of the extraordinary "light harvesting" capability of the polymer host and the high quantum yield of the dye molecules, the fluorescence brightness of the perylene- and coumarin-doped nanoparticles is estimated to be $\sim$200 times larger than that of single quantum dots and 40 times higher than that of dye-loaded silica spheres of similar dimensions. The combination of the high

brightness, highly red-shifted emission spectrum, and excellent photostability is promising for biological labeling and sensing applications.

4. Conclusions

Fluorescent dye-doped polyfluorene nanoparticles were prepared by a reprecipitation method, and energy transfers between the host polymer and the guest molecules were studied by steady state and time-resolved fluorescence measurements. A combined energy diffusion and Förster transfer model was determined to adequately describe the energy transfer efficiency in the doped nanoparticles. Energy transfer in the dye-doped nanoparticles was found to improve photostability, resulting in photostability estimated to be hundreds or thousands of times larger than dyes in solution. Fluorescence quantum yields of ~40% and a peak extinction coefficient of 1.5×10^9 $M^{-1}cm^{-1}$ were determined for aqueous suspensions of ~30 nm diameter polymer nanoparticles doped with perylene or coumarin 6 (2 wt %). The combination of high brightness, highly red-shifted emission spectrum, and excellent photostability are promising for fluorescence imaging and multiplexing applications.

Acknowledgment. We gratefully acknowledge financial support from the NSF/EPSCoR under Grants No. 2001RII-EPS-0132573 and 2004RII-EPS-0447660, NSF CAREER Grant No. CHE-0547846, and NIH Grant No. 1R01GM081040.

References and Notes

(1) Förster, T. *Ann. Phys.* **1948**, *2*, 55.
(2) Ha, T.; Zhuang, X. W.; Kim, H. D.; Orr, J. W.; Williamson, J. R.; Chu, S. *Proc. Natl. Acad. Sci. U.S.A.* **1999**, *96*, 9077.
(3) Medintz, I. L.; Clapp, A. R.; Mattoussi, H.; Goldman, E. R.; Fisher, B.; Mauro, J. M. *Nature Mater.* **2003**, *2*, 630.
(4) Berggren, M.; Dodabalapur, A.; Slusher, R. E.; Bao, Z. *Nature* **1997**, *389*, 466.
(5) Friend, R. H.; Gymer, R. W.; Holmes, A. B.; Burroughes, J. H.; Marks, R. N.; Taliani, C.; Bradley, D. D. C.; Dos Santos, D. A.; Bredas, J. L.; Loglund, M.; Salaneck, W. R. *Nature* **1999**, *397*, 121.
(6) Pei, Q. B.; Yang, Y. *J. Am. Chem. Soc.* **1996**, *118*, 7416.
(7) Scherf, U.; List, E. J. W. *Adv. Mater.* **2002**, *14*, 477.
(8) Gong, X.; Wang, S.; Moses, D.; Bazan, G. C.; Heeger, A. J. *Adv. Mater.* **2005**, *17*, 2053.
(9) Chen, L. C.; Roman, L. S.; Johansson, D. M.; Svensson, M.; Andersson, M. R.; Janssen, R. A. J.; Inganas, O. *Adv. Mater.* **2000**, *12*, 1110.
(10) Gong, X.; Ma, W. L.; Ostrowski, J. C.; Bazan, G. C.; Moses, D.; Heeger, A. J. *Adv. Mater.* **2004**, *16*, 615.
(11) Cabanillas-Gonzalez, J.; Fox, A. M.; Hill, J.; Bradley, D. D. C. *Chem. Mater.* **2004**, *16*, 4705.
(12) Mahajan, N. P.; Linder, K.; Berry, G.; Gordon, G. W.; Heim, R.; Herman, B. *Nat. Biotechnol.* **1998**, *16*, 547.
(13) Ha, T.; Enderle, T.; Ogletree, D. F.; Chemla, D. S.; Selvin, P. R.; Weiss, S. *Proc. Natl. Acad. Sci. U.S.A.* **1996**, *93*, 6264.
(14) Clapp, A. R.; Medintz, I. L.; Mauro, J. M.; Fisher, B. R.; Bawendi, M. G.; Mattoussi, H. *J. Am. Chem. Soc.* **2004**, *126*, 301.
(15) Xu, Q. H.; Wang, S.; Korystov, D.; Mikhailovsky, A.; Bazan, G. C.; Moses, D.; Heeger, A. J. *Proc. Natl. Acad. Sci. U.S.A.* **2005**, *102*, 530.
(16) Chen, L.; McBranch, D. W.; Wang, H. L.; Helgeson, R.; Wudl, F.; Whitten, D. G. *Proc. Nat. Acad. Sci. U.S.A.* **1999**, *96*, 12287.
(17) Fan, C. H.; Wang, S.; Hong, J. W.; Bazan, G. C.; Plaxco, K. W.; Heeger, A. J. *Proc. Nat. Acad. Sci. U.S.A.* **2003**, *100*, 6297.
(18) Wu, C.; Szymanski, C.; McNeill, J. *Langmuir* **2006**, *22*, 2956.
(19) Wu, C.; Peng, H.; Jiang, Y.; McNeill, J. *J. Phys. Chem. B* **2006**, *110*, 14148.
(20) Jang, S. J.; Newton, M. D.; Silbey, R. J. *Phys. Rev. Lett.* **2004**, *92*, 218301.
(21) Bruchez, M.; Moronne, M.; Gin, P.; Weiss, S.; Alivisatos, A. P. *Science* **1998**, *281*, 2013.
(22) Chan, W. C. W.; Nie, S. M. *Science* **1998**, *281*, 2016.
(23) Michalet, X.; Pinaud, F. F.; Bentolila, L. A.; Tsay, J. M.; Doose, S.; Li, J. J.; Sundaresan, G.; Wu, A. M.; Gambhir, S. S.; Weiss, S. *Science* **2005**, *307*, 538.
(24) Ow, H.; Larson, D. R.; Srivastava, M.; Baird, B. A.; Webb, W. W.; Wiesner, U. *Nano Lett.* **2005**, *5*, 113.
(25) Wang, L.; Wang, K. M.; Santra, S.; Zhao, X. J.; Hilliard, L. R.; Smith, J. E.; Wu, J. R.; Tan, W. H. *Anal. Chem.* **2006**, *78*, 646.
(26) Derfus, A. M.; Chan, W. C. W.; Bhatia, S. N. *Nano Lett.* **2004**, *4*, 11.
(27) Kirchner, C.; Liedl, T.; Kudera, S.; Pellegrino, T.; Javier, A. M.; Gaub, H. E.; Stolzle, S.; Fertig, N.; Parak, W. J. *Nano Lett.* **2005**, *5*, 331.
(28) Ego, C.; Marsitzky, D.; Becker, S.; Zhang, J. Y.; Grimsdale, A. C.; Mullen, K.; MacKenzie, J. D.; Silva, C.; Friend, R. H. *J. Am. Chem. Soc.* **2003**, *125*, 437.
(29) Tong, A. K.; Li, Z. M.; Jones, G. S.; Russo, J. J.; Ju, J. Y. *Nat. Biotechnol.* **2001**, *19*, 756.
(30) Wang, L.; Tan, W. *Nano Lett.* **2006**, *6*, 84.
(31) Szymanski, C.; Wu, C.; Hooper, J.; Salazar, M. A.; Perdomo, A.; Dukes, A.; McNeill, J. D. *J. Phys. Chem. B* **2005**, *109*, 8543.
(32) Eggeling, C.; Widengren, J.; Rigler, R.; Seidel, C. A. M. *Anal. Chem.* **1998**, *70*, 2651.
(33) Morris, V. J.; Kirby, A. R.; Gunning, A. P. *Atomic force microscopy for biologists*; Imperial College Press: London, 1999.
(34) Yang, Z. Q.; Huck, W. T. S.; Clarke, S. M.; Tajbakhsh, A. R.; Terentjev, E. M. *Nat. Mater.* **2005**, *4*, 486.
(35) Virgili, T.; Lidzey, D. G.; Bradley, D. D. C. *Adv. Mater.* **2000**, *12*, 58.
(36) Lyons, B. P.; Wong, K. S.; Monkman, A. P. *J. Chem. Phys.* **2003**, *118*, 4707.
(37) Pschenitzka, F.; Sturm, J. C. *Appl. Phys. Lett.* **1999**, *74*, 1913.
(38) Peng, A. D.; Xiao, D. B.; Ma, Y.; Yang, W. S.; Yao, J. N. *Adv. Mater.* **2005**, *17*, 2070.
(39) Zhong, G. Y.; He, J.; Zhang, S. T.; Xu, Z.; Xiong, Z. H.; Shi, H. Z.; Ding, X. M.; Huang, W.; Hou, X. Y. *Appl. Phys. Lett.* **2002**, *80*, 4846.
(40) Jakabovic, J.; Lengyel, O.; Kovac, J.; Wong, T. C.; Lee, C. S.; Lee, S. T. *Appl. Phys. Lett.* **2003**, *83*, 1295.
(41) Rettig, W.; Majenz, W. *Chem. Phys. Lett.* **1989**, *154*, 335.
(42) Lakowicz, J. R. *Principles of Fluorescence Spectroscopy*; Plenum Press: New York, 1999.
(43) Becker, K.; Lupton, J. M. *J. Am. Chem. Soc.* **2006**, *128*, 6468.
(44) Campoy-Quiles, M.; Heliotis, G.; Xia, R. D.; Ariu, M.; Pintani, M.; Etchegoin, P.; Bradley, D. D. C. *Adv. Funct. Mater.* **2005**, *15*, 925.
(45) Jones, G.; Jackson, W. R.; Choi, C.; Bergmark, W. R. *J. Phys. Chem.* **1985**, *89*, 294.
(46) Lyons, B. P.; Monkman, A. P. *Phys. Rev. B* **2005**, *71*, 235201.
(47) Halls, J. J. M.; Pichler, K.; Moratti, S. C.; Holmes, A. B. *Appl. Phys. Lett.* **1996**, *68*, 3120.
(48) Markov, D. E.; Amsterdam, E.; Blom, P. W. M.; Sieval, A. B.; Hummelen, J. C. *J. Phys. Chem. A* **2005**, *109*, 5266.
(49) Rosenstock, H. B. *Phys. Rev.* **1969**, *187*, 1166.
(50) Powell, R. C.; Soos, Z. G. *Phys. Rev. B* **1972**, *6*, 4035.
(51) Gamertsfelder, G. R.; Goldhaber, M. *Phys. Rev.* **1942**, *62*, 556.
(52) Stevens, M. A.; Silva, C.; Russell, D. M.; Friend, R. H. *Phys. Rev. B* **2001**, *63*, 165213.
(53) Haugeneder, A.; Neges, M.; Kallinger, C.; Spirkl, W.; Lemmer, U.; Feldmann, J.; Scherf, U.; Harth, E.; Gugel, A.; Mullen, K. *Phys. Rev. B* **1999**, *59*, 15346.
(54) Press, W. H.; Teukolsky, S. A.; Vetterling, W. T.; Flannery, B. P. *Numerical Recipes in C*; Cambridge University Press: Cambridge, 1988.
(55) Herz, L. M.; Silva, C.; Grimsdale, A. C.; Mullen, K.; Phillips, R. T. *Phys. Rev. B* **2004**, *70*, 165207.
(56) Yan, M.; Rothberg, L. J.; Papadimitrakopoulos, F.; Galvin, M. E.; Miller, T. M. *Phys. Rev. Lett.* **1994**, *73*, 744.
(57) List, E. J. W.; Guentner, R.; de Freitas, P. S.; Scherf, U. *Adv. Mater.* **2002**, *14*, 374.
(58) Ariu, M.; Lidzey, D. G.; Sims, M.; Cadby, A. J.; Lane, P. A.; Bradley, D. D. C. *J. Phys.: Condens. Matter* **2002**, *14*, 9975.
(59) Widengren, J.; Rigler, R. *Bioimaging* **1996**, *4*, 149.
(60) Zondervan, R.; Kulzer, F.; Kol'chenko, M. A.; Orrit, M. *J. Phys. Chem. A* **2004**, *108*, 1657.
(61) Schindler, F.; Lupton, J. M.; Feldmann, J.; Scherf, U. *Adv. Mater.* **2004**, *16*, 653.